Binary Neutron Star Systems: Analysis of simulated data to understand their evolution

Andrea Nicolai, Camilla Quaglia, Sandeep Kumar Shekhar and Walter Zigliotto

Department of Physics and Astronomy
Università degli Studi di Padova
via 8 Febbraio 1848, 2, 35122 Padova PD

Abstract

The aim of this work is to understand the formation of the sources of gravitational waves, in particular the formation of binary neutron stars. Data used is simulated by MOBSE. The analysis considers binary neutron stars systems that merge within a Hubble time. In addition, this work gives an overview about the nature of their physical properties such as masses of progenitors, mass of Compact Objects formed, type and number of Common Envelopes and finally delay time densities for varying metallicities and fMTs.

Keywords: Binary Neutron Stars, Data, Compact Objects, Common Envelopes, metallicities, fMT.

1. Introduction

The Einstein's general theory of relativity revolutionized the field of physics[1]. The theory relates the curvature in space-time with the energy of the object. The Einstein equation is given as:

$$R_{\alpha\beta} - \frac{R}{2} g_{\alpha\beta} = \frac{8\pi G}{c^4} T_{\alpha\beta} \tag{1}$$

Where, $R_{\alpha\beta}$ is the Ricci tensor, R is the Ricci scalar, $g_{\alpha\beta}$ is the metric and $T_{\alpha\beta}$ is the stress energy tensor. The linearised field equations (expanded as a perturbation of the flat space-time Lorentz metric) had the form of a relativistic wave equation with the space-time perturbation propagating as a wave (so-called ripples of geometry) moving at the speed of light. The

propagating field was a second order tensor field which in vacuum has the form $\Box^2\phi_{\alpha\beta} = 0$[2] ($\Box$ is the d'alembertian operator), i.e.,

$$\frac{\partial^2\phi_{\alpha\beta}}{\partial t^2} - \frac{1}{c^2}\nabla^2\phi_{\alpha\beta} = 0 \tag{2}$$

Where, ϕ is the scalar field and ∇ is the Laplace operator. Gravitational waves were detected in the year 2015[3]. The waves were the result of the merger of Binary Black Holes (BBH). Several events have been detected in the recent past[4, 5, 6]. Previously cited references are the waves from the BBH. Our work involves the evolution of Binary Neutron Stars (BNS). The coalescence of BNS was first observed in the year 2017[7] and the electromagnetic counterpart was observed as short Gamma Ray Burst (GRB), with a delay of $+1.74 \pm 0.05$s[8, 9]. Jocelyn Bell Burnell and Antony Hewish discovered pulsars in 1967[10], which were later identified as rapidly rotating NS. NS are astronomical objects with densities roughly of the order of $10^{17}-10^{18}kgm^{-3}$[11, 12], roughly 10^8 times higher than that of a white dwarf. The NS's that exists in nature are found to be $< 3M_\odot$. There has been a lot of development in the nuclear theory describing the internal constituents of the NS in the recent years. The constraints placed on the Equation of State (EoS) of NS determines the mass of the NS. Maximum mass of NS is altogether a new topic of study, the constraints involving the quarks[13], f(R) gravity[14], presence of dark matter particles[15]. LIGO-VIRGO collaborations have also been involved in understanding the nature of these compact binaries.

Our work involves to understand the binary progenitor stars evolution which results in a the formation of BNS. We observe more than 55% of the stars in our galaxy are binary and multiple stars[16]. The progenitor stars that form NS are in the mass range of $\sim 9 - 20M_\odot$. All stars undergo main sequence phase, characterised by core hydrogen burning, and spend 90% of their lifetime in the hydrogen burning phase. The hydrogen burning timescale for a $13M_\odot, 15M_\odot, 20M_\odot$ star is around $13, 11, 8$ million years respectively[17]. One of the salient features of stellar evolution is the mass loss. Stars lose mass at all evolutionary stages, including the main sequence. The rates of mass loss vary, however, over a very wide range. Thus, the mass loss rate is so slow as to have a discernible effect on the stellar mass The solar wind, for example, removes the mass from the Sun at a rate of $\sim 10^{-14}M_\odot yr^{-1}$[18].

1.0.1. ***Mass Transfer***

In the binary systems, mass transfer occurs between the stars by three prominent mechanisms:

- Wind transfer
- Roche Lobe Overflow (RLO)
- Common Envelope (CE)

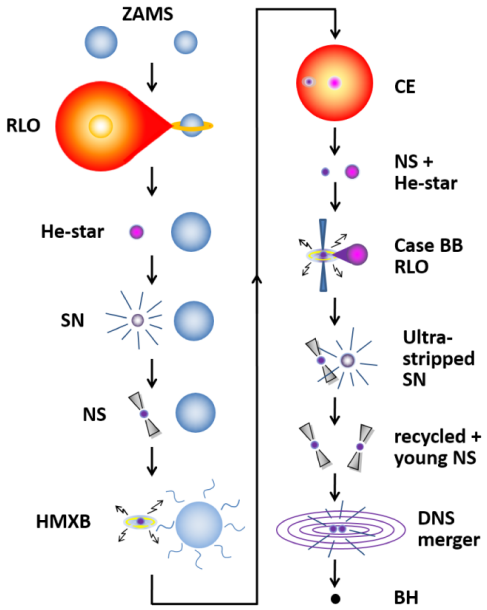

Figure 1: A typical formation channel of the BNS[19]. ZAMS:Zero Age Man Sequence, RLO: Roche Lobe Overflow, He-star: Helium-star, SN: Supernova, HMXB: High Mass X-Ray Binary, CE: Common Envelope, DNS: Double Neutron Star.

Wind transfer

The primary progenitor (larger of the two) loses mass by stellar winds.The stellar winds in very massive stars is due to the coupling through resonant metal lines, hence making it explicitly dependent on metallicity. Metallicity in the stars is again dependent on the Initial Mass Function (IMF). The secondary accretes the mass lost as stellar winds from the primary and is given as[20]:

$$\frac{|\dot{M}_{2A}|}{|\dot{M}_{1W}|} \propto \left(\frac{v_{orb}}{v_W}\right)^4 \tag{3}$$

Where, $\dot{M}_{2A}$ is the mass accreted by the secondary, $\dot{M}_{1W}$ represents the mass loss due to the stellar winds from the primary and v_W is the wind velocity. This model is deemed as an inefficient way to describe the mass transfer. There has been a significant development to find an ideal model for mass loss through stellar winds.

Roche Lobe Overflow

The BNS formation involves the primary progenitor exhausting hydrogen burning in the core and the outer layers of the star to expand (Red Giant Phase). The secondary progenitor accretes the outer expanded layers of the primary star, leading to a mass gain. This process results in a Roche-Lobe Overflow (RLO). There exists a equipotential points in binary system and are called Lagrangian points (L1, L2, L3, L4). These Lagrangian points separate the lobes. When the primary stars' outer layer radius becomes greater or equal to the inner most Lagragian point (L1), mass transfer occurs to the secondary star. This phenomenon is known as Roche lobe overflow. The effective radius (R_L) is given as[21]:

$$\frac{R_L}{a} \approx \frac{0.49q^{\frac{2}{3}}}{0.6q^{\frac{2}{3}} + ln(1 + q^{\frac{1}{3}})} \tag{4}$$

Where $q = m1/m2$ and a is the orbital separation. RLO continues if $q > 1$ and i.e., $m1 > m2$. During this span the orbital separation sinks between the stars. Once the masses are equalized and $m1 < m2$ the orbital separation and donor's roche lobe increase.

Common Envelope

A common envelope is usually formed when one of the star is a compact object in a binary star system and the other star expands rapidly[22]. The donor star will start mass transfer when it overfills its Roche lobe and as a consequence the orbit will shrink further causing it to overflow the Roche lobe even more, which accelerates the mass transfer, causing the orbit to shrink even faster and the donor to expand more. This leads to the run-away process of dynamically unstable mass transfer. In some case the receiving star is unable to accept all material, which leads to the formation of a common

envelope engulfing the companion star[23].

Fig.1 depicts a summary of typical BNS formation. The binary progenitors are in the ZAMS phase. One of the stars exhaust hydrogen burning in the core and expand the outer layers filling the roche lobes. The secondary star accretes matter from the primary. The primary explodes as a supernova and a compact core is left behind. The NS can accrete matter from the secondary and emit X-rays. The secondary's outer envelope encloses the primary NS and mass is accreted by the NS. If the common envelope is ejected, the binary system is retained. The secondary star undergoes supernova and leaves behind a NS. The primary and the secondary NS form a tight binary and finally merge to either a NS or a BH.

1.0.2. ***fMT***

fMT is a parameter that determines the mass transfer efficiency. It plays a prominent role in deciding the fate of the binaries. If the accretor is a non-degenerate star, then fMT is represented as:

$$\dot{M}_{accretor} = fMT(|\dot{M}_{donor}|) \tag{5}$$

In case the accretor is a compact object, then fMT is:

$$\dot{M}_{accretor} = fMT(|\dot{M}_{donor}|)(|\dot{M}_{Edd}|) \tag{6}$$

2. Methods

The major focus of our study is on the statistical analysis of a large number of BNS systems through simulated data. This analysis has been pursued using Python 3.7.7, in particular numpy 1.18.1 and pandas 1.0.3 libraries. Data that is stored in a external server has been accessed remotely by the mean of a VPN.

MOBSE (Massive Objects in Binary Stellar Evolution) is a simulated population synthesis code, developed by Hurley as BSE[24] and upgraded by Giacobbo, Mapelli and Spera[25], with the aim of investigating the evolution of binary stellar systems. In particular, MOBSE takes into account of metallicity-dependent prescriptions for stellar winds, the dependency of mass loss on the electron-scattering Eddington factor of the star, and new

solutions for core-collapse SN.

For this analysis, the dataset, generated through MOBSE, consists of about a billion binary systems of isolated massive binaries over a Hubble time. The prominent features are metallicity (Z), Roche lobe mass transfer efficiency (fMT) and the parameter α, that expresses the dependence of mass loss on metallicity. These features are set as:

- Z : 0.02, 0.016, 0.012, 0.008, 0.006, 0.004, 0.002, 0.0016, 0.0012, 0.0008, 0.0004 and 0.0002.
- fMT: 1, 0.7, 0.5, 0.4, 0.3, 0.2 and 0.1.
- α : 5.

Furthermore, data is collected into 5 chunks for computing optimization. According to them, directories are split in a tree structure (Fig.2), where each chunks contains the following files: $COB.out$, $CO.out$, $evol\_mergers.out$, $failed\_systems.out$, $input$, $mergers.out$, $params.out$ and src.

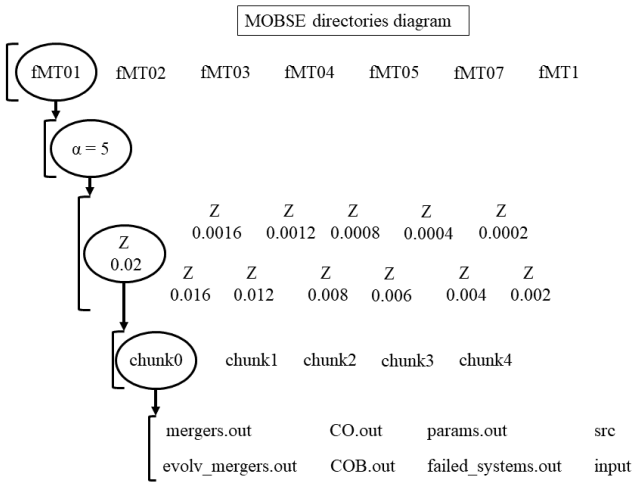

Figure 2: Schematic representation of block directories.

Nevertheless, the study concentrates on three of them:

- $mergers.out$: Contains information on compact objects binaries that merge in a Hubble time.

- *evolv_mergers.out*: Contains detailed information on each binary system evolution (e.g. Fig.3).
- *COB.out*: Contains the output of all compact objects that form.

Moreover, the values of mass, luminosity and radius are expressed in solar units, while the time is expressed in Myr units. Each of the aforementioned dataset includes many parameters. The main parameters taken into account are:

- ID: Identification number of the binary system.
- $k1$, $k2$: Type of the star. The algorithm's stellar types corresponds to the evolutionary phases sketch by the rapid SSE (Single Star Evolution) code[24].
- m_1, m_2: Mass of the star, where m_1 is identified as the star coming from the most massive progenitor.
- *t_step*: The current time of the system.
- *label*: Information on the current status of the binary system.
- *sep*: The current semi-major axis separation.

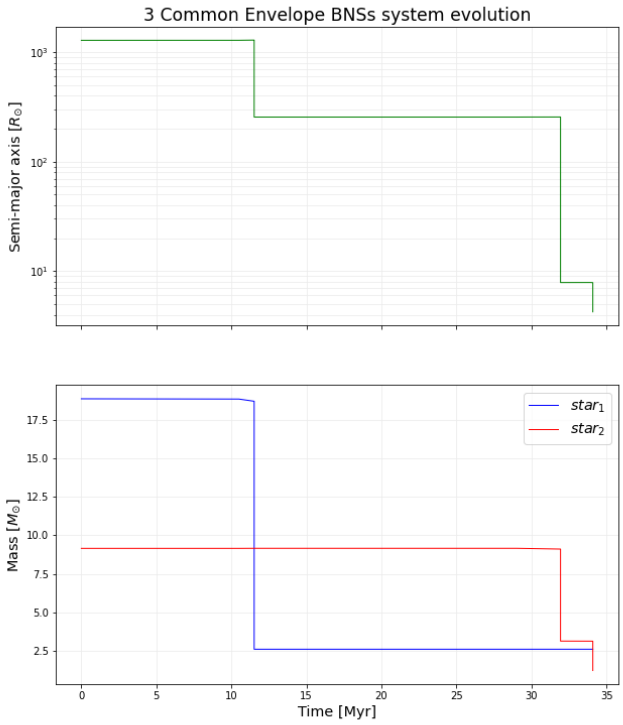

Figure 3: Common envelope time evolution system.

3. Results

Binary compact objects systems may or may not merge within a Hubble time. The analyzed data takes account of the both cases. We can count the number of merging systems, normalized to the total number of binary systems generated by MOBSE simulation. Generally, for higher values of fMT we have lower fraction of merging systems, although for high metallicities this trend strongly reverses as seen in the left side of Fig.4. This occurs in a flex point which is around $Z \sim 0.006$. Moreover a local minimum is observed around $Z \sim 0.0015$.

In order to understand the process that leads to low merging system at $fMT = 1$ and low Z, it is assumed that the number of BNS are almost the

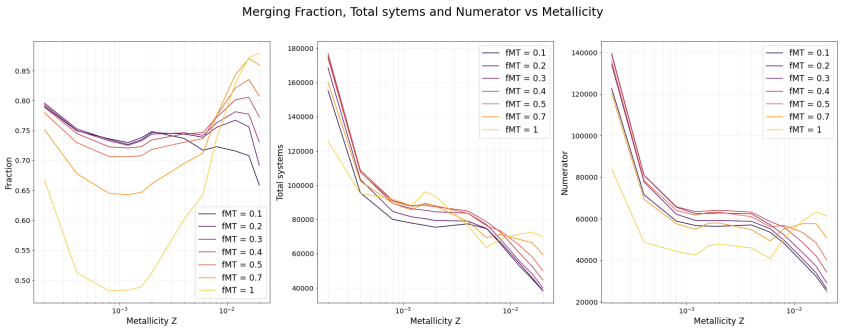

Figure 4: Left: Fraction of merging systems with respect to the total number. Centre: Total number of systems. Right: Number of merging systems.

same for all the fMT's, as shown in the Fig.4(middle plot). On the other hand, when fMT is very low, binary star systems tend to evolve into BNS. For higher fMT value, binary star systems tend to evolve into BBH. In fact, with low fMT, a smaller fraction of the mass loss by the more massive primary star is accreted by the secondary star, thereby the primary ending up as a NS. An efficient mass transfer from the primary to the secondary will result as a latter becoming a BH. Therefore, with high fMT, one can expect a higher probability for a NSBH formation. Furthermore, at $Z \sim 10^{-3}$ the theory of stellar evolution highlights the stellar radii to be comparatively larger than at other values of metallicity, especially during the red giant phase. At high metallicity (e.g., solar metallicity) the system is expected to lose mass efficiently due to stellar winds, thereby unable to have larger radius. On the contrary for lower metallicity, the star is compact with respect to the intermediate metallicity. This is primarily because of the higher temperature in the core, enabling it to "burn" higher amount of fuel and end its life relatively early without losing much mass. Interestingly, at $Z \sim 10^{-3}$ the stars have a striking balance between the percentage of metals and the mass loss. There are several constraints involved for the formation of BNS based on the distance between the binaries. If the progenitor binaries are too close, during the CE phase, the binaries might merge producing a massive star or a BH, because of the large radii of the stars. In case the binaries are too far away, we do not expect them to merge in the Hubble time.

3.1. ***Merging System***

Our analysis is focused on the systems that merge within a Hubble time by the emission of gravitational waves, further we shall consider the ones that can easily be done with no error, (included in a specific database). Furthermore, only systems that end up with BNSs are taken into account.

3.1.1. ***Compact Objects Binary Masses***

The Fig.5 highlights the different mass variation between the total non conservative and strictly conservative systems. For $fMT = 0.1$ the massive progenitors are viable. This is due to the fact that the largest star loses considerably more mass which is not accreted by the secondary. For such instance, the secondary star is likely to evolve into a NS rather than a BH. With $fMT = 1$ the Δm_2 systems are generally shifted at lower side. We expect the secondary's mass not to vary significantly from the progenitor star,because of the accretion of matter from the primary progenitor (during the red giant phase). Furthermore, with high value of fMT a number of BNS mergers are lost. Currently, we do not have a good understanding of it. To conclude, Fig.5 shows that it is possible to end up forming NSs, from massive progenitors $(15 - 25 M_{\odot})$. This again is majorly dependent on fMT and Z. In fact, higher Z increases Δm due to the effect of stellar winds.

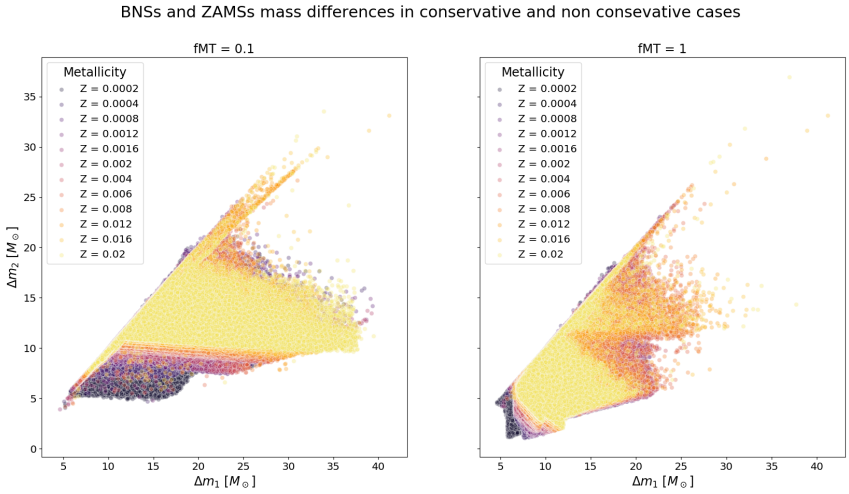

Figure 5: Difference between progenitor's mass and and the NS's mass. On the left fMT = 0.1 and on the right fMT = 1.

The normalized histograms of masses for the two Compact Objects (CO) that form the binary are produced, for varying Z and fMT, where the primary is more massive than the secondary, $m1 > m2$. In the Fig.6 the histograms for solar metallicity, $Z = 0.02$, and for $Z = 0.0004$ are shown. We notice that for lower metallicities the density (i.e. the number of counts) decreases. One reason for this discrepancy is the role of winds. Massive progenitors with lower metals retains most of its mass (absence of winds). Hence the CO left behind has higher mass, exceeding the TOV limit[26, 27] and collapse to a BH. From both the plots, the distribution peaks around $1.2M_{\odot}$, as expected for a NS. Also, we observe a second peak, which is due to the existence of NS's from the electron capture supernovae. As the fMT value increases the density of NS occurrence from electron capture supernovae increases; it is suppressed for $fMT = 0.1$. This phenomenon exists for stars with an initial mass between 7 and 10 $M_{\odot}$, and this is why the second distribution in Fig.7 doesn't show this behaviour. The latter is strongly peaked at the same value like in the primary mass distribution (Fig.6). The mass of the secondary is almost entirely left by core collapse supernovae.

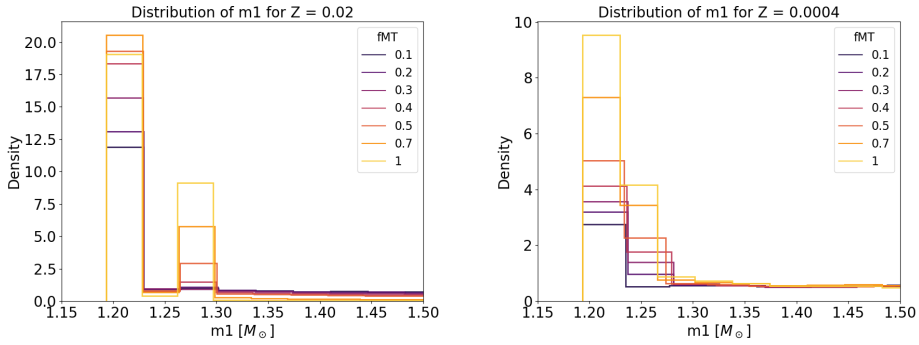

Figure 6: Distribution of the first CO's mass.

Moreover the distribution of the mass ratio q between the secondary and the primary CO is shown in the Fig.8, this time for fixed fMT and varing Z. For $fMT = 1$ the value of q strongly peaks around 1 and the number of counts is directly proportional to metallicity. Interestingly, this behaviour is true also for smaller values of fMT.

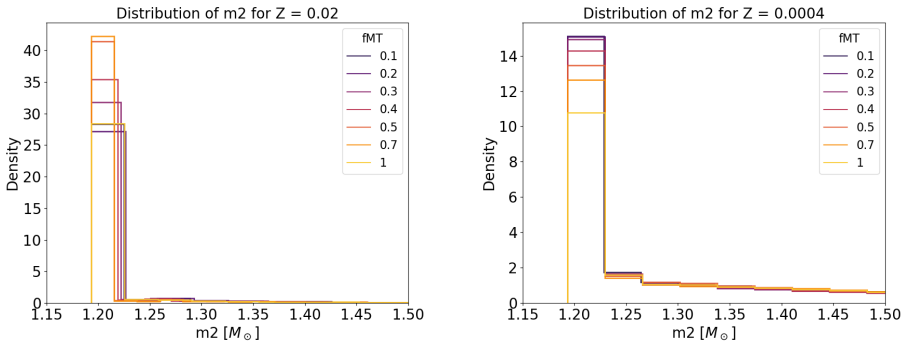

Figure 7: Distribution of the second CO's mass.

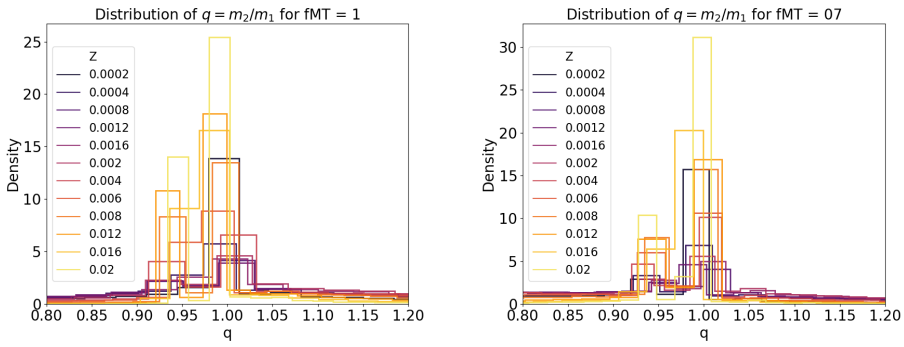

Figure 8: Distribution of the mass ratio for $fMT = 1$ and $fMT = 0.7$.

The distribution of the mass differences between m_1 and m_2 and the respective ZAMS masses, from which the COs are formed, are shown in the Fig.9, for solar metallicity and $Z = 0.0004$. We notice that for higher values of fMT the mass difference is smaller; this behaviour is typical for different metallicities. From this plot we restate that it is possible to have NS from more massive progenitors than expected. On the other hand, for an isolated star to form NS from a progenitor more massive than about $20M_\odot$ is not feasible. Also, through the comparison between $Z = 0.02$ and $Z = 0.0004$, we notice that as Z increases the minimum mass to form a NS tends to shift more to the right.

To verify if the mass of the NS originating from the most massive progenitor is effectively larger than the mass of the other NS, the fraction of flipped

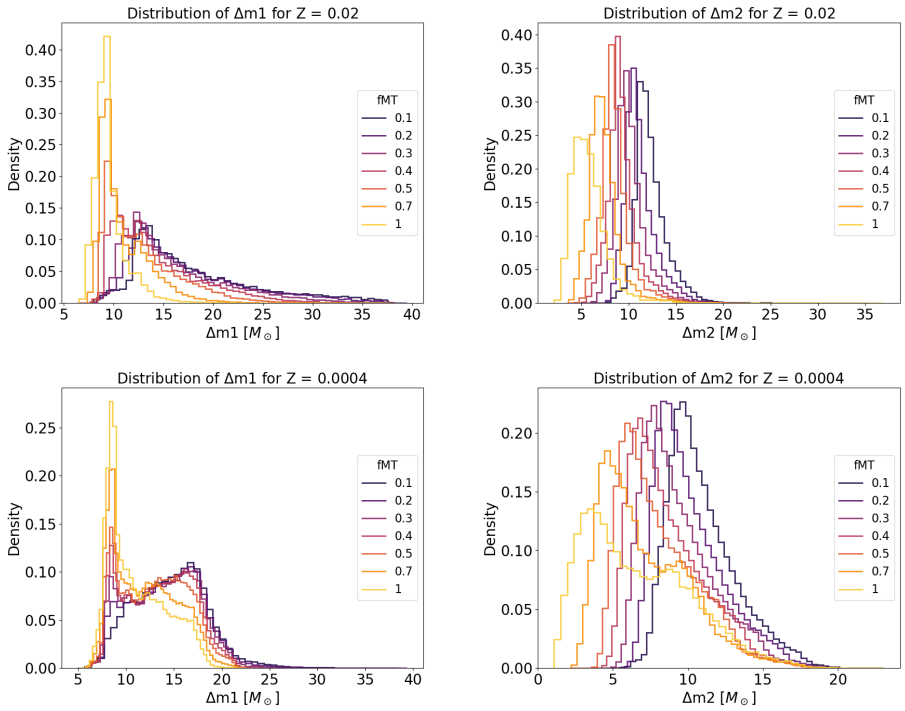

Figure 9: Distribution of the mass difference between the first and second CO and their progenitor star, for $Z = 0.02$ and $Z = 0.0004$.

masses between the primary and the secondary is plotted in Fig.10, as a function of fMT. From this plot, it is clear that for more efficient mass transfer, the fraction of flipped mass increases.

3.1.2. ***Delay times - power law coefficient***

Delay time in gravitational wave astronomy is defined as the time taken by the massive compact objects to coalesce, on-sight of formation.
In order to avoid the need of running the entire simulation for obtaining a set of delay times, we would want to estimate a global parameter that certainly should help us in describing BNS population. By this way we will be able to meaningfully sample from the selected population, and consequently analyze delay times.
As we can see from the density graph in log-log scale (Fig.11a), the density of delay times follows a linear behavior. The estimation of its coefficient for all the systems, and the dependence on fMT and Z, using as time bounds from

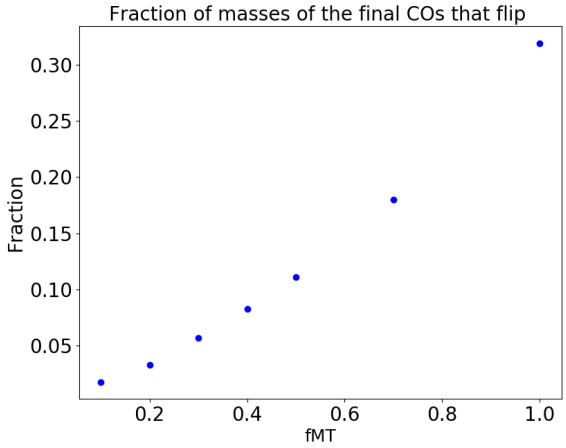

Figure 10: Plot of the fraction of the systems that presents flipped masses of the final COs with respect to the progenitors.

10^2 to $10^4 Myr$ is done. This procedure is quite handy to take into account only the linear part, thus neglecting the tails. Since we are considering the log-log scale, the original framework density of time delays obeys a power law of the kind:

$$y(x) = b \cdot x^a$$

The coefficient a needs to be estimated, which is the slope returned by the linear regression.
Results of the fit are depicted in Fig.11b. These values are computed by the mean of the method 'polyfit' in the Python library 'numpy', that returns the regression line coefficients and errors given by the least squares algorithm.

These results show the exponent to be dependent on Z. Higher the mass transfer efficiency, the more probable is to have a larger delay times at exponent being least, and the tail distribution becoming more relevant. Generally, this is valid up to $Z \sim 0.006$, where this behaviour reverses: the curve indeed changes concavity and we can consider at that particular metallicity as an inflection point.
However, it is to be noted as the a coefficient clusters around a certain value, we can therefore estimate its weighted mean taking into account of all values that is obtained so far:

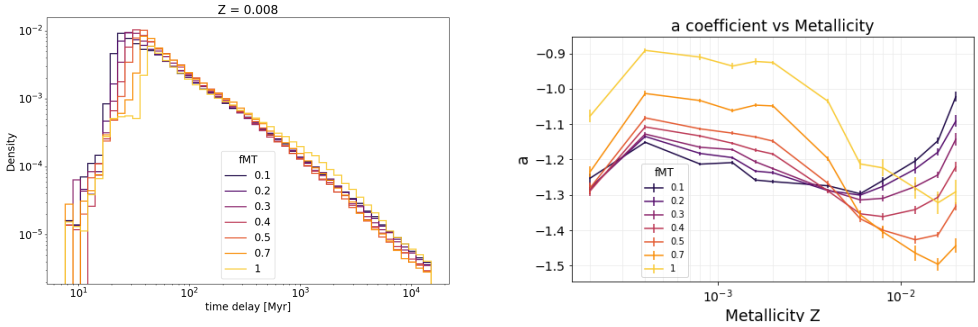

(a) Distribution of delay times in log scale: since density is linear, a linear fit is used and the coefficients computed.

(b) Coefficient 'a' found for the slope of the density histograms as the function of the metallicity. Errors are found by the mean of the linear regression algorithm.

Figure 11: Basic analysis for the 'a' coefficient.

$$a = -1.24 \pm 0.13 \quad Myr^{-1} \tag{7}$$

3.1.3. ***Common Envelope phase***

Another important subject is whether the system taken into account experiences a Common Envelope (CE) phase (briefed in the introductory section). When we analyze and look into the considered data, every system is associated with a label denoting the phase of evolution. The label 'COMENV' refers to a CE phase just ended, which may be physically true or not. Thus we consider only the former, i.e., the ones that do not appear in the same line of the database of a previously formed BNS system. Whereas, the hypothetical ones refer to a "cheat" of the simulation code, and are not to be taken into account.

In our work we have primarily considered if a CE phase exists or not. Thanks to the following result Fig.12, one can see that the fraction of system that does not go through the CE phase is statistically irrelevant. This is the raison d'être for our analysis, by means of grouping binary systems based on the number of CE it goes through, assuming that one being the least. The existence of CE is highly characteristic feature of BNS systems. It is very unlikely to find the formation of BNS systems without a single CE phase in nature.

3.2. ***Common Envelope - numbers***

Speaking in terms of statistics, the systems that do not undergo CE phase are judged as irrelevant in our analysis. Generally, there is a possibility of CE phase occurring more than once for a single system. The number of CE phases can reach up to three in number. We split our events according to this count, and finally normalize it to the total systems. Curves describing these fraction as function of Z and efficiency of mass transfer are shown in the Fig.12.

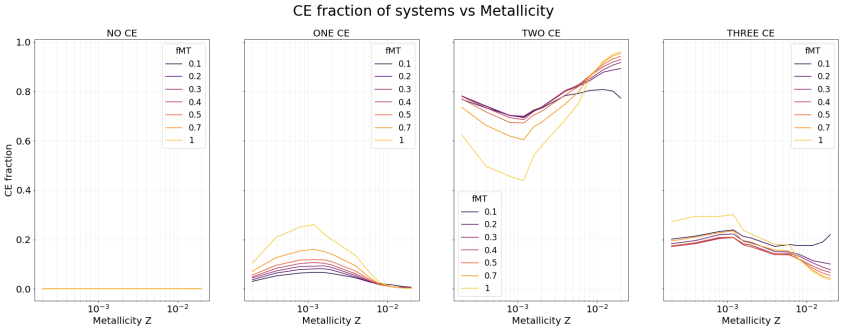

(a)

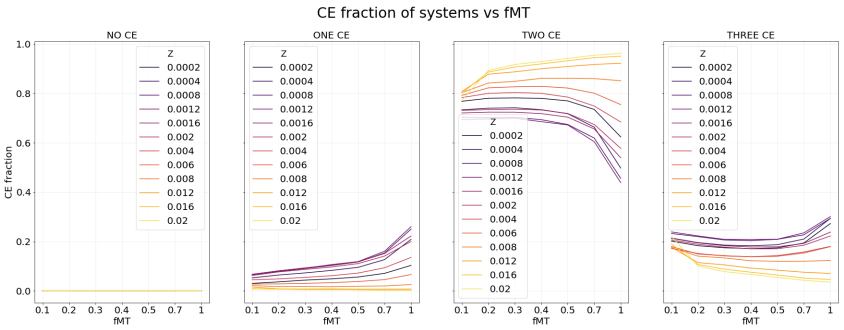

(b)

Figure 12: Fraction of systems and corresponding number of CE for different Z and fMT.

One can easily notice that almost every system experiences at least one CE phase during its lifetime. More likely to face two CEs. There is an important feature to be noted: the increase in Z and fMT leads to the increase of the CE fraction as shown in the Fig.12, namely favoring two CE phases formation. For one CE and three CE phase is actually the contrary effect (low

Z and low fMT). Another interesting feature for all the curves in Fig.15c, there exists a stationary point around $Z \sim 0.001$.

3.2.1. ***Types of CE***

We label our CE phase according to all possible cases in which it might occur. The combination is represented as:

- **1A** star + star → star' + star'
- **1B** star + star → NS + star'
- **1C** star + star → NS + NS
- **2A** NS + star → NS + star'
- **2B** NS + star → NS + NS

Where *star* is referred to a star that is yet to become a NS.

It is interesting to analyze a few special cases for systems where only a single, as well as two or three, CEs occur. Here all the possible combinations for the CE to occur given by their number for a certain system are produced.

The Fig.13a gives us information about the types of CEs formed. The systems with one CE are said to have higher probability of one of the binary to be a NS to have already been formed. Moreover, higher the metallicity, the lesser number of systems with two stars experience a CE ($1A, 1B, 1C$ type, darker colors in the plots). Additionally, the largest number of CEs are related to low metallicities for all fMTs. Also, we notice a change in behaviour after the point $Z \sim 0.006$. For low fMTs, CE events decrease, whereas for higher values it increases. This might be because of ineffective mass transfer by not filling the Roche lobes, CE fails to occur or is comparatively quite low. Finally, we infer that there is almost no statistics for **1C** type, therefore it is highly unlikely for two stars to experience a CE and both of them turning out to be BNS. Despite the lack of statistics, it is still an interesting topic for future works. Since these kind of systems exist, one would definitely like to investigate them.

An initial remark about Fig.13b is by considering systems with two CE, we are indeed taking into the majority of systems for our database. This

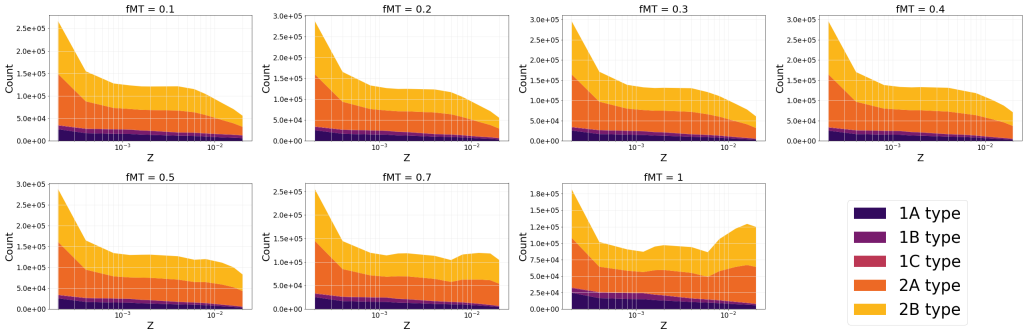

(a) Count of CE grouped per type, given only ONE has occurred.

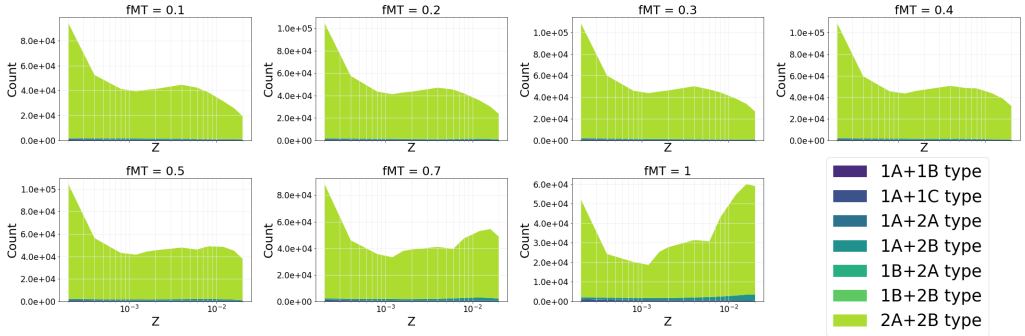

(b) Count of CE grouped per type, given TWO have occurred.

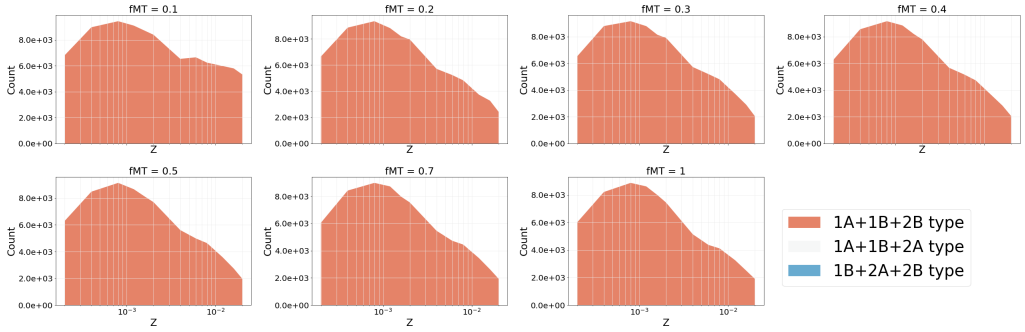

(c) Count of CE grouped per type, given THREE have occurred.

Figure 13: Plots depicting the different number of CEs, type, or combination of types, is more likely to occur. Scale is chosen not to be log-log one in order to visualize data in a better and clearer way: The larger is the area related to a single color, the more a specific type of CE is observed.

is concluded by the courtesy of Fig.12. One may note that almost all the statistics is covered by the combination of types referring to CE occurring with a NS already formed. A possible interpretation for the case where the system goes through two CE is more likely. These might be the following reasons: once the primary progenitor is already a NS, the secondary may go through the first CE therefore ejecting its hydrogen envelope if the spiraling has sufficient energy to do so. At this moment simulation takes into account the change of phase for the second object, and we are left with a binary system where the first object is already a NS and the second one is a Wolfrayet star (WR). After a short time compared to star's lifespan, but sufficiently large for a WR, there exists a non null probability that the helium layer of the secondary object is ejected as well, forming the second Common Envelope. The plot (Fig.14) therefore endorses our hypothesis.

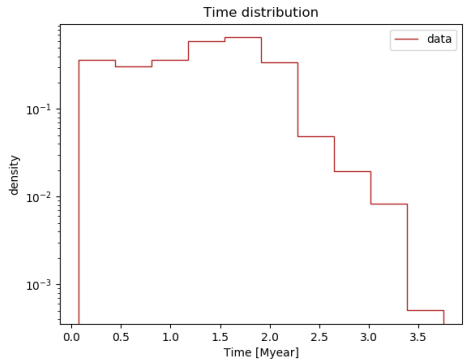

Figure 14: Histogram for times spent between two consecutive 2A and 2B CEs.

According to Fig.13b, we observe a strong change in behavior after $Z \sim 0.006$, depending on fMT. For low fMT total number of events counted decreases, instead for $fMT \geqslant 0.5$ it first flattens and then increases. For metallicities lower than $Z \sim 0.006$ point, graphs do not show any higher variation. For high mass transfer efficiency, probability of CE between two stars that may change type and finally not ending up as a NS, is seen to slightly increase, but still being negligible with respect to the other cases.
However, Fig.13c shows out of the the five possible CE combination, the one where two stars change type after a CE phase is $1A$. Hence one of them becomes a NS ($1B$) and finally the last CE leads its companion to become a NS itself ($2B$). For ($2A$, $2B$) the same reason is valid as stated before,

therefore $2A$ and $2B$ may refer to two CEs one shortly after the other one (see fig 14). For three events of CE, we observe that the behavior is unique for every fMT parameter, except for 0.1, where we count a larger number of events. This is indeed coherent with the result previously obtained in Fig.12a.

3.2.2. ***Power law coefficient***

A similar analysis method is used as previously done in a previous section. Due to the fact that log-log density plot of the delay times is linear, a similar analysis technique is pursued and the coefficient a for different values of the number of CEs is counted.

An interesting feature from Fig.15a is systems with only one 'CE' data noisy when compared, but still assumed to be a near to "flat" distribution. In-spite of the low statistics, we can nevertheless state that systems with a single CE is more likely to have either a very small delay time, or a very large one. Indeed the a coefficient (Fig.15b), for low metallicites, is related to this subset of data and is collocated around 0 which is the slope and is expected from the plots. Other plots, present in the GitHub [28], describes this "noisy" behavior for high Z. In the region around $Z \sim 0.006$, there is a notable change in behavior of the curve. On the other hand for two and three CEs, curves are very similar and coherent one to each other. Once more we stress the value $Z \sim 0.006$ to be region specific, where especially for the graph in the center, lines cross each other. Finally, there are three CE phases curves that almost coincide.

From the previous plot (Fig.15c), we determine that for low metallicities a coefficient is independent of fMT. Whereas, it is a sensible change go higher with Z, and its values are different. The reason for this can be explained by the mean of (Fig.12): For high Z we see that very few systems do only one CE, so the statistic is low in order to estimate a correctly. This comes in handy as to tell us why there is a discontinuity for high Z and for a few values of a are either missing or are sparser. Physically, it would mean that the system undergoes a single CE, then delay times will tend be larger. Note that a discontinuity, (i.e., a lack of value in the plot), is due to the non convergence of the algorithm used in order to make the linear regression. Contributions by small metallicities may return a positive value for the a coefficient, that in turn would make the distributions of delay time be peaked towards even higher times.

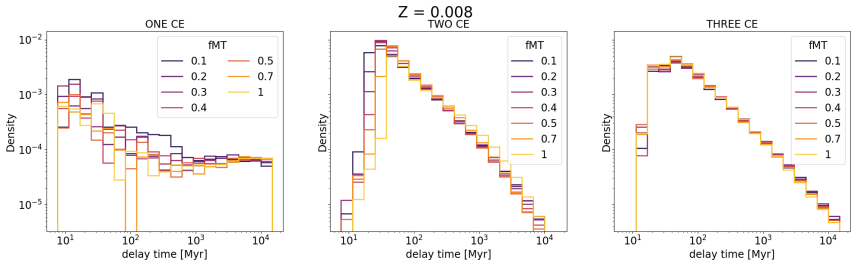

(a) Density of delay times in log-log scale for different numbers of CEs.

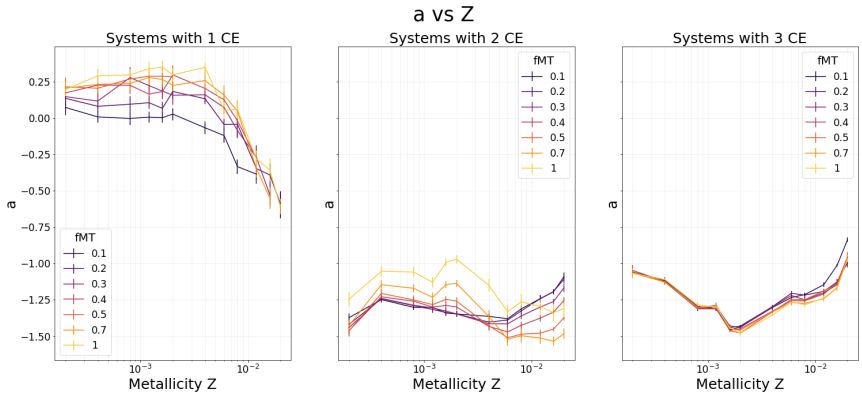

(b) Coefficient a is found for the slope of the density histograms as the function of Z. Errors are found by the mean of the linear regression algorithm.

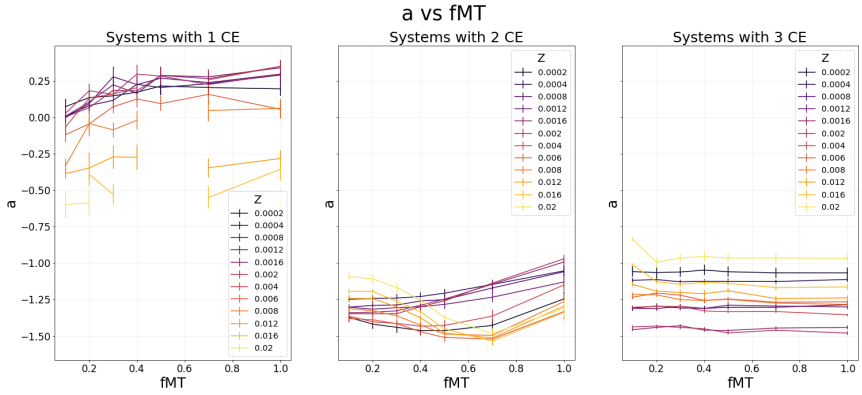

(c) Coefficient a is found for the slope of the density histograms in function of the fMT. Errors are found by the mean of the linear regression algorithm.

Figure 15: Basic analysis for the a coefficient.

Putting the pieces together, we summarise our result into the following table 1 for systems with different numbers of CE:

	1 CE	**2 CE**	**3 CE**
a coefficient $[Myr^{-1}]$	0.01 ± 0.27	-1.31 ± 0.13	-1.19 ± 0.15

Table 1: Table depicting the value of the a coefficient for the power law related to delay times density. Values are computed by using weighted mean and its error.

As already mentioned that delay times for one CE systems are way larger, this might be due of the lack of statistics related to those systems, or eventually to the physics hiding behind this phenomenon that is to be investigated thoroughly. The first hypothesis is more probable according to the uncertainty which is almost doubled for one CE systems.

3.2.3. ***Mass density scatter-plots***

Based on the number of CE's that a system might undergo, we obtain the scatter plot for the masses m_1 and m_2.
We choose as initial masses the ones in the database with label *'INITIAL'* and are considered to be at time zero (clearly for systems that end up being BNS). Therefore, we consider the masses of their progenitors. Final masses are those of the compact objects.

According to the Fig.16a, mass distribution of systems that experience one CE phase are highly concentrated between $15M_\odot - 20M_\odot$. The BNSs formed are from the massive progenitors. But, this inference deviates from the established theory of stellar evolution. Distribution for one CE is relatively broader than the two and three CE. Generally, for higher masses, we tend to have only one CE, while for masses around $(10 - 12M_\odot, 8 - 10M_\odot)$ either two or three. These are relatively low masses, and according to Fig.12a are the most statistically relevant systems in our population[29, 30]. For almost equal masses, namely for points lying on the bisector line, there is a possibility of the system undergoing three CE.

The Fig.(16b) suggests a discontinuity in the scatter plots. The probably because of the bug in the code. We recognize a general trend in the number of CEs a system goes through with respect to its masses "flipped" (compact objects generated by the most massive progenitor become the least massive ones). If the systems undergoes a higher number of CEs, then the

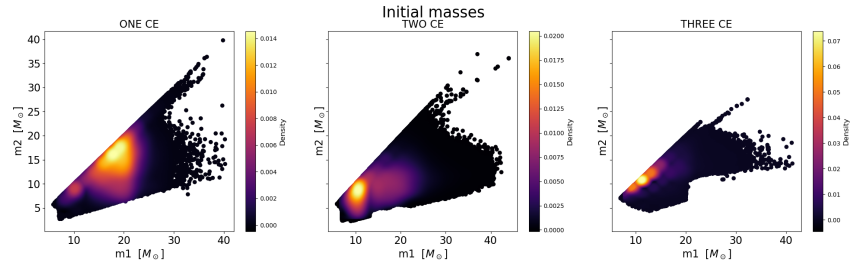

(a) Scatter density plot:Initial mass 1 and mass 2 of the progenitors for all fMT and all Z.

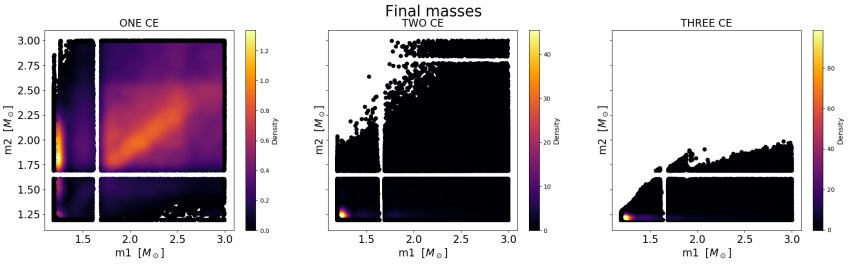

(b) Scatter density plot:Final mass 1 and mass 2 of the NS before merger for all fMT and all Z.

Figure 16: Scatter density plots of masses of progenitors and compact objects generated after them.

probability of its masses being flipped is low. In addition, increasing the number of CE, it can be seen that the majority of systems tend to lie in the "lower right" half of the plot, this is the locus of points where $m_1 \geqslant m_2$ and therefore masses do not flip. Moreover, when the system goes through two or three CE, more likely is the masses of the compact objects that is left behind.

Our focus is now on the effect of CE's on the primary NS. According to Fig.16b for two and three CE, the primary NS seems to be peeled off as well. Indeed they do not appear to be massive, as it happens for the one CE scatterplot in the top-right box. This is due to a selection effect. We need to recall that according to MOBSE simulator a CE phase may occur when the mass ratio between the donor and the accretor is above a certain threshold. This is due to several number of parameters taken into account for Mass Transfer time-scale instability in the real world. The justifications are by some correlations between the scale for instability of Mass Transfer and critical values for mass ratio q. However, this result sets a limit for the second CE to occur. If as an example: the primary object is quite massive ($\sim 2M\odot$), it is unusual for the secondary to have a mass, such that it is

above the q-critical threshold, after being peeled out from its hydrogen outer layer.

As pointed out previously, the major results are in Fig.(16). We would like to take the coordinates in unit of $(m_1[M\odot], m_2[M\odot])$ of the densest bins for every fMT and Z, Assuming that it characterizes our systems. It is important to see how these coordinates change for different fMT, number of CEs, and Z varying. This is done for both initial masses (Fig.17) and final masses (Fig. 18).

According to the Fig.17, the most common systems going through one CE tend to have higher m_1 and m_2 with respect to the other cases, while ratio between initial masses slightly differs from 1. Moreover, points are sparser than others and no general pattern can be easily identified. This is coherent to what we have found previously in Fig.16a. Note that for the mass conservative case, the most probable systems tend to cluster towards least massive ones. This may be due to the fact that the resulting compact objects, being the total mass preserved, are more likely to collapse into BHs.

The last consideration is about the points related to three CE that lie on the bisector line (i.e., the locus of points where the two masses are equal). Higher the metallicity, the more massive are the progenitors.

Note as for final masses (fig. 18), there is no dependence on fMT and Z for systems that go though 2 and 3 CE, beside stochastic oscillations. For these systems stellar winds are totally irrelevant, and so dependence on Z and fMT is lost. The same results could have been deduced also from fig. (6) and fig. (7). This can either be treated as a problem of the simulation, that almost deterministically returns compact objects with a certain mass, or we may find a physical explanation for this to occur. However, in nature, masses of already observed neutron stars follow a broader distribution [31], making us endorse the first hypothesis. Therefore MOBSE needs a revision and further development when NS are produced in binary systems, specially regarding their masses.

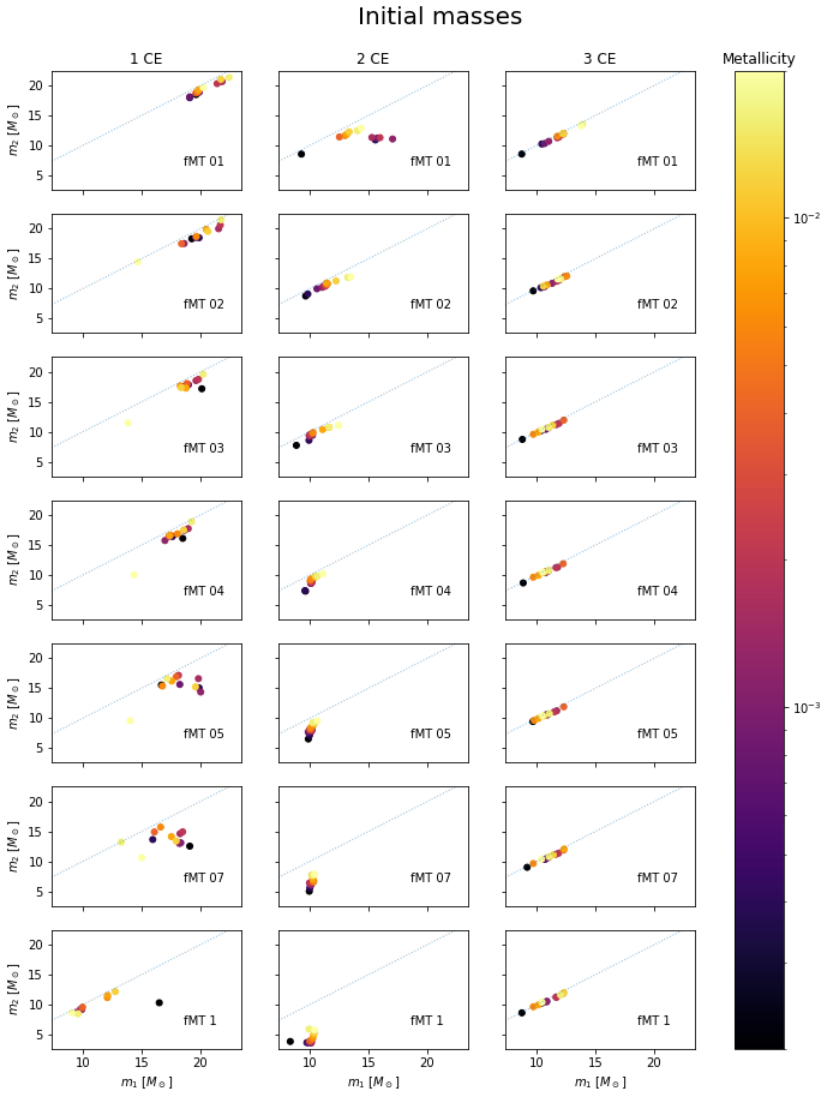

Figure 17: Curves describing the coordinates of densest bins, in terms of the masses of the progenitors m_1 and m_2. The bisector line where the two masses are equal is visible.

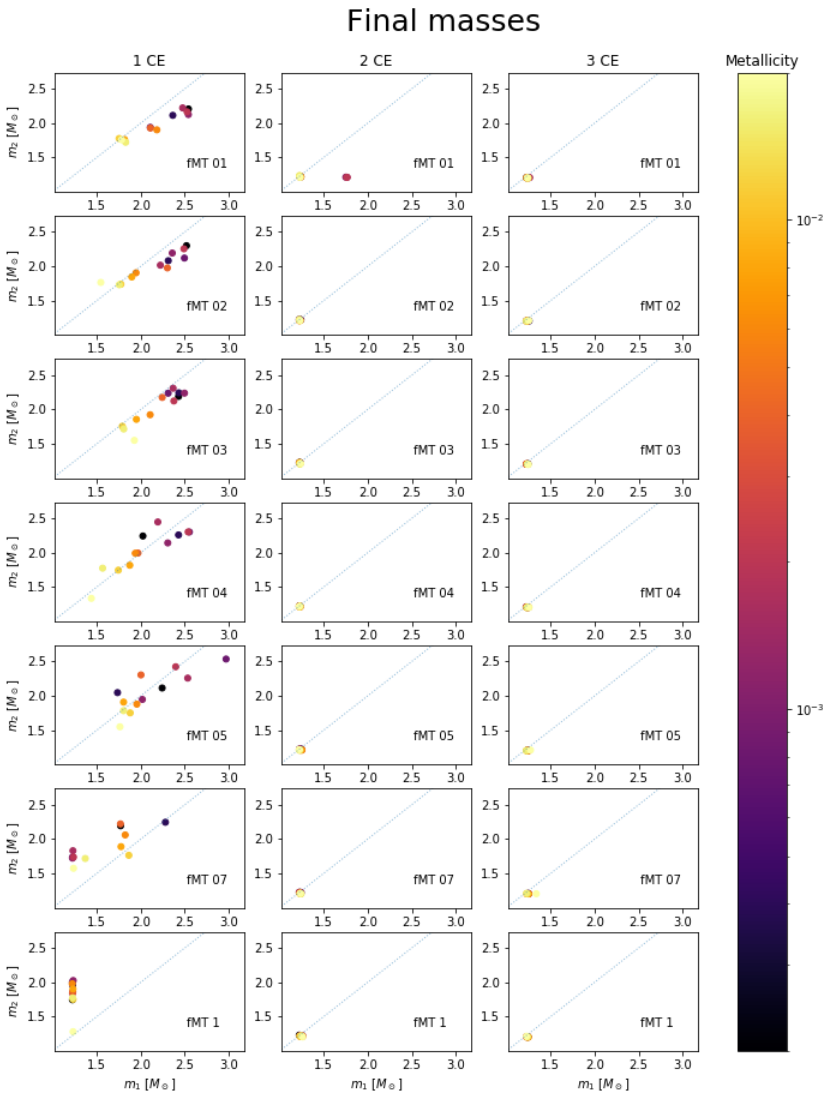

Figure 18: Curves describing how the coordinates of densest bins, in terms of the masses of the progenitors m_1 and m_2. Bisector line where the two masses are equal is visible.

4. Conclusions

In this work we have analyzed the output of the MOBSE simulation, primarily focused on the binary systems which might evolve into NS. Taking into account the fraction of merging systems with respect to the total number, we have noticed that the number of systems that merge is dependent on Z and fMT (Fig.4). In the future we shall investigate the merging fraction of binary NS-BH systems and its behavior with respect to fMT and Z and compare it with BNSs.

Further, we have considered only systems that merge within a Hubble time, and plotted the difference in mass units between progenitor masses and COs formed (Fig.5) to discover the possibility of high massive progenitors ending up as BNSs. Interestingly, preliminary histogram analysis of distribution of masses for both the NS that would form, we have spotted the presence of the NS formation by the process of electron capture supernovae (Fig.6).

In addition, we have understood how the density plots for delay times follow, in $log-log$ scale, a linear law (Fig.11) and computed the slope of the latter. Later, we considered systems by grouping them by number and type (Sec.3.2.1) of CEs they go through. The delay times power law coefficient has been computed as well by distinguishing systems based on the number of CE they go through.

Finally, we have considered both the masses of the progenitors by grouping them by number of CE and the compact objects they would form (Fig.16). The density and the coordinates are plotted, in terms of m_1 and m_2, of the densest bin (Fig.17 18). The nature of these plots shown are to be studied in the future. On the contrary, we might have pointed out a problem of MOBSE, whose masses of compact object are not distributed as found in the nature, and therefore a revision is suggested.

References

[1] A. Einstein, The Foundation of the General Theory of Relativity, Annalen Phys. 49 (1916) 769–822.

[2] A. Einstein, Über Gravitationswellen, Sitzungsberichte der Königlich Preußischen Akademie der Wissenschaften (Berlin (1918) 154–167.

[3] B. Abbott, et al. (LIGO Scientific, Virgo), Observation of Gravitational Waves from a Binary Black Hole Merger, Phys. Rev. Lett. 116 (2016) 061102. doi:10.1103/PhysRevLett.116.061102.

[4] B. Abbott, et al. (LIGO Scientific and Virgo Collaboration), GW170104: Observation of a 50-solar-mass binary black hole coalescence at redshift 0.2, Phys. Rev. Lett. 118 (2017) 221101. doi:10.1103/PhysRevLett.118.221101.

[5] B. Abbott, et al. (LIGO Scientific and Virgo Collaboration), GW170608: Observation of a 19 solar-mass binary black hole coalescence, The Astrophysical Journal 851 (2017) L35. doi:10.3847/2041-8213/aa9f0c.

[6] B. Abbott, et al. (LIGO Scientific and Virgo Collaboration), GW170814: A three-detector observation of gravitational waves from a binary black hole coalescence, Phys. Rev. Lett. 119 (2017) 141101. doi:10.1103/PhysRevLett.119.141101.

[7] B. Abbott, et al. (LIGO Scientific and Virgo Collaboration), GW170817: Observation of gravitational waves from a binary neutron star inspiral, Phys. Rev. Lett. 119 (2017) 161101. doi:10.1103/PhysRevLett.119.161101.

[8] B. Abbott, et al. (LIGO Scientific and Virgo Collaboration), Gravitational waves and gamma-rays from a binary neutron star merger: GW170817 and GRB170817a, The Astrophysical Journal 848 (2017) L13. doi:10.3847/2041-8213/aa920c.

[9] A. Goldstein, et al., An ordinary short gamma-ray burst with extraordinary implications: Fermi-GBM detection of GRB 170817a, The Astrophysical Journal 848 (2017) L14. doi:10.3847/2041-8213/aa8f41.

[10] A. Hewish, S. J. Bell, J. D. H. Pilkington, P. F. Scott, R. A. Collins, Observation of a rapidly pulsating radio source, nat 217 (1968) 709–713. doi:10.1038/217709a0.

[11] J. B. Hartle, A. G. Sabbadini, The equation of state and bounds on the mass of nonrotating neutron stars., apj 213 (1977) 831–835. doi:10.1086/155214.

[12] I. Goldman, S. Nussinov, Weakly interacting massive particles and neutron stars, Phys. Rev. D 40 (1989) 3221–3230. doi:10.1103/PhysRevD.40.3221.

[13] F. Weber, M. Meixner, R. P. Negreiros, M. Malheiro, Ultra-Dense Neutron Star Matter, Strange Quark Stars, and the Nuclear Equation of State, Int. J. Mod. Phys. E 16 (2007) 1165–1180. doi:10.1142/S0218301307006599.

[14] S. Capozziello, M. De Laurentis, R. Farinelli, S. D. Odintsov, Mass-radius relation for neutron stars in $f(r)$ gravity, Phys. Rev. D 93 (2016) 023501. doi:10.1103/PhysRevD.93.023501.

[15] S. S. Kumar, A. Kenath, C. Sivaram, Effects of dark matter on the upper bound mass of neutron stars, Physics of the Dark Universe 28 (2020) 100507. doi:https://doi.org/10.1016/j.dark.2020.100507.

[16] H. Sana, S. de Mink, A. de Koter, N. Langer, C. Evans, M. Gieles, E. Gosset, R. Izzard, J.-B. Bouquin, F. Schneider, Binary interaction dominates the evolution of massive stars, Science 337 (2012) 444. doi:10.1126/science.1223344.

[17] S. E. Woosley, A. Heger, T. A. Weaver, The evolution and explosion of massive stars, Rev. Mod. Phys. 74 (2002) 1015–1071. doi:10.1103/RevModPhys.74.1015.

[18] D. Prialnik, An Introduction to the Theory of Stellar Structure and Evolution, 2009.

[19] T. M. Tauris, M. Kramer, P. C. C. Freire, N. Wex, H.-T. Janka, N. Langer, P. Podsiadlowski, E. Bozzo, S. Chaty, M. U. Kruckow, E. P. J.

van den Heuvel, J. Antoniadis, R. P. Breton, D. J. Champion, Formation of double neutron star systems, The Astrophysical Journal 846 (2017) 170. doi:10.3847/1538-4357/aa7e89.

[20] H. Bondi, F. Hoyle, On the Mechanism of Accretion by Stars, Monthly Notices of the Royal Astronomical Society 104 (1944) 273–282. doi:10.1093/mnras/104.5.273.

[21] P. Eggleton, Evolutionary Processes in Binary and Multiple Stars, Cambridge Astrophysics, Cambridge University Press, 2006. doi:10.1017/CBO9780511536205.

[22] J. I. Icko, M. Livio, Common envelopes in binary star evolution, Publications of the Astronomical Society of the Pacific 105 (1993) 1373. doi:10.1086/133321.

[23] N. Ivanova, S. Justham, J. L. Avendano Nandez, J. C. Lombardi, Identification of the Long-Sought Common-Envelope Events, Science 339 (2013) 433. doi:10.1126/science.1225540.

[24] J. R. Hurley, C. A. Tout, O. R. Pols, Evolution of binary stars and the effect of tides on binary populations, Monthly Notices of the Royal Astronomical Society 329 (2002) 897–928. doi:10.1046/j.1365-8711.2002.05038.x.

[25] N. Giacobbo, M. Mapelli, M. Spera, Merging black hole binaries: the effects of progenitor's metallicity, mass-loss rate and Eddington factor, Monthly Notices of the Royal Astronomical Society 474 (2017) 2959–2974. doi:10.1093/mnras/stx2933.

[26] R. C. Tolman, Static solutions of einstein's field equations for spheres of fluid, Phys. Rev. 55 (1939) 364–373. doi:10.1103/PhysRev.55.364.

[27] J. R. Oppenheimer, G. M. Volkoff, On massive neutron cores, Phys. Rev. 55 (1939) 374–381. doi:10.1103/PhysRev.55.374.

[28] WASC, Mobse - bns systems, 2020. URL: https://github.com/andrybicio/MOBSE_BNS.

[29] P. Kroupa, On the variation of the initial mass function, Monthly Notices of the Royal Astronomical Society 322 (2001) 231–246. doi:10.1046/j.1365-8711.2001.04022.x.

[30] E. E. Salpeter, The Luminosity Function and Stellar Evolution., apj 121 (1955) 161. doi:10.1086/145971.

[31] N. Farrow, X.-J. Zhu, E. Thrane, The mass distribution of galactic double neutron stars, The Astrophysical Journal 876 (2019) 18. URL: https://doi.org/10.3847%2F1538-4357%2Fab12e3. doi:10.3847/1538-4357/ab12e3.